Food Hydrocolloids 141 (2023) 108673

Contents lists available at ScienceDirect

Food Hydrocolloids

journal homepage: www.elsevier.com/locate/foodhyd

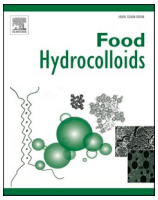

Physicochemical properties, structural characteristics and *in vitro* digestion of brown rice–pea protein isolate blend treated by microbial transglutaminase

Lin Zhao [a], Ming-Hsu Chen [b,c], Xuezhi Bi [d,e], Juan Du [a,*]

[a] Food, Chemical and Biotechnology Cluster, Singapore Institute of Technology, 10 Dover Drive, Singapore, 138683, Singapore
[b] School of Chemical and Biomedical Engineering, Nanyang Technological University, 62 Nanyang Drive, Singapore, 637459, Singapore
[c] Institute of Food Science and Technology, National Taiwan University, No. 1, Sec. 4, Roosevelt Rd, Taipei, 10617, Taiwan
[d] Bioprocessing Technology Institute (BTI), Agency for Science, Technology and Research (A*STAR), Singapore, 138668, Singapore
[e] Duke-NUS Medical School, National University of Singapore, Singapore, 169857, Singapore

ARTICLE INFO

Keywords:
Plant-based protein
Microbial transglutaminase
Functional property
Protein structure
In vitro digestion
Amino acid release

ABSTRACT

The present study sought to use microbial transglutaminase (MTG) to modulate the physicochemical properties of brown rice protein isolate (BRPI), pea protein isolate (PPI) and their blend, and determine MTG's effect on protein structural and digestive profile changes. MTG at concentration of 1 U/g significantly increased water holding capacity (91.6% enhancement) and decreased oil holding capacity (39.3% reduction) of BRPI + PPI (4:6) blend, respectively, accompanied by decreasing their solubility and zeta potential values in aqueous system. From rheological analysis, MTG-induced crosslinks could result in stronger and more elastic gels in BRPI + PPI blend with lower gel point temperature. SDS-PAGE demonstrated that the number and intensities of the protein bands for all MTG-treated BRPI were similar under both non-reducing and reducing conditions, whereas in the samples containing PPI, fewer and fainter bands were shown in the groups treated by MTG at concentration of 4 U/g and above. From FTIR spectra, lower level of random coils paralleled by an increase in both β-sheet structures and α-helix band were observed in the 1.0 U/g MTG-treated BRPI + PPI blend, indicating the protein-protein interactions within the mixed systems might boost the role of MTG in the structural modification, facilitating the network formation of more ordered structure with better thermal stability. Results of *in vitro* digestion showed less hydrophobic amino acids and essential amino acids including Lys released in MTG-treated BRPI + PPI blend's digests. Overall, the application of MTG in plant-based proteins can potentially contribute to the development of innovative food products with modified functionalities and unique digestive characteristics.

1. Introduction

Proteins derived from animal sources are gradually replaced with plant-based proteins in recent years, driven by health-conscious consumers and a series of ecological and environmental concerns (Nasrabadi, Doost, & Mezzenga, 2021). Currently a variety of plant-based proteins, e.g., soy, wheat, pea, corn and cottonseed proteins, have been widely used in food industry as dietary supplements or nutritional ingredients (Kumar et al., 2022), but studies related to the development of brown rice protein-based food product are limited. Brown rice protein is regarded as a valuable plant protein source due to its hypoallergenic property and richness in essential amino acids. Nevertheless, it exhibits low solubility, pH susceptibility, and poor surface-active properties in aqueous systems, which can be constraints in food applications (Agboola, Ng, & Mills, 2005). Therefore, finding an effective way to improve functionalities of brown rice protein is of great significance in developing a novel plant-based food product, and using microbial transglutaminase (MTG) could be one choice.

MTG (EC 2.3.2.13) is a protein-glutamine γ-glutamyl-transferase, which can catalyse crosslinking of proteins by forming ε-(γ-glutamyl)-lysine (G-L) bond between the γ-carboxyamide group of glutamine (Gln, acyl donor) and the ε-amino group of lysine (Lys, acyl acceptor) residues in proteins (Wang et al., 2020). Since MTG has been regarded as Generally Recognised as Safe (GRAS) by Food and Drugs Administration (FDA) in 1998, it has been widely used in food industry to provide foods with improved and/or innovative attributes that can meet the demand

* Corresponding author.
E-mail address: du.juan@singaporetech.edu.sg (J. Du).

https://doi.org/10.1016/j.foodhyd.2023.108673
Received 20 October 2022; Received in revised form 3 March 2023; Accepted 11 March 2023
Available online 16 March 2023

of consumers. The studies related to MTG application in several food systems, e.g., dairy, bakery, meat and fish products, have been well reported for its unique performance in facilitating protein polymerisation and modifying protein functional properties (Dube, Schäfer, Neidhart, & Carle, 2007; Renzetti, Behr, Vogel, & Arendt, 2008). However, little attention was paid to MTG's effects on physicochemical property, protein structural and digestive profile changes of brown rice protein, especially when combined with pea protein to produce protein-enriched foods with better amino acid balance.

It has been well believed that the combination of legumes and cereals could complement each other in nutritional value, as the former contains high level of Lys that is lacking in the latter, whereas the latter is rich in methionine, an essential amino acid the former is inadequate (Ikujenlola & Fashakin, 2005). Moreover, in the presence of MTG, the addition of Lys-rich legume proteins to cereal proteins might facilitate the formation of new protein crosslinks catalysed by MTG, changing physicochemical properties of the blends and extending the use of both two proteins. For example, Bonet, Blaszczak, and Rosell (2006) incorporated several legume proteins like soy and lupin flour into wheat dough under MTG treatment, discovering heterologous structures formed in the wheat-lupin blends accompanied by modified thermal behaviour.

To the best of our knowledge, the enzymatic modification effect of MTG on brown rice protein isolate (BRPI) coupled with pea protein isolate (PPI) has not been studied sufficiently. Pea protein has been receiving the growing attention in the market in recent years due to its low allergenicity and rich nutritional profile (Jiang et al., 2017). Therefore, pea protein was chosen in this study, hoping it can offer a great complementary function to brown rice protein under MTG treatment. The main objective of this research was to explore the action mechanisms of MTG on the structure-function relationships of BRPI + PPI blends, by investigating the impact of MTG on physicochemical properties, protein profiles and secondary structure of this mixture. Moreover, the digestive performance of MTG-treated protein blends was also studied via the *in vitro* digestion model and nuclear magnetic resonance (NMR) spectroscopy, with primary focus on the releases of amino acids during digestion, to determine MTG's effect on amino acid bioavailability and the nutritional quality of the proteins. The discoveries gained from this study could give us a new insight into the nature of the interaction within plant protein blends after MTG treatment, serving as a basis for better MTG utilisation in the development of new and improved plant-based food products in the future.

2. Materials and methods

2.1. Materials

Brown rice protein isolate (BRPI, containing ≥80% protein (d.b.), manufactured by Xi'an BIOF Bio-Technology Co., Ltd (China)), was purchased from Agrocorp (Singapore). Pea protein isolate (PPI, containing ≥80% protein (d.b.)), was supplied by HA LI FA Pte Ltd (Singapore). The proximate compositions of BRPI and PPI, including protein, moisture, fat, carbohydrate and ash were documented in the Certificate of Analysis supplied by the vendors and shown in the Supplementary (Table S1). Food grade microbial transglutaminase (MTG) from *Streptoverticillium mobaraense* (2500 U/g, manufactured by Jiangsu Zipin Biotech Co., Ltd (China)), was purchased from MegaChem Ltd (Singapore). The canola oil used in oil holding capacity analysis was purchased from local supermarket.

For *in vitro* digestion, α-amylase (EC 3. 2. 1. 1, 12 U/mg) isolated from porcine pancreas, pepsin (EC 3. 4. 23. 1, 3940 U/mg) isolated from porcine gastric mucosa, pancreatin (EC 232. 468. 9, a mixture of several digestive enzymes including amylase, trypsin, lipase, ribonuclease and protease; 96.7 U/mg on the basis of trypsin activity) isolated from porcine pancreas, bile extract, and other chemical reagents (analytical grade) were all purchased from Sigma-Aldrich Pte Ltd (Singapore).

2.2. Preparation of MTG-modified proteins

One gram of BRPI, PPI and their blend was dispersed in 10 mL of MTG solution (pH 7, prepared in 10 mM acetate buffer with a final concentration of 0.5 U/g protein and 1.0 U/g protein, respectively) or 10 mL of 10 mM acetate buffer (pH 7, for control group), respectively. The concentrations of MTG used in our study were determined after considering the production efficiency and cost in practical food industry. After mixed thoroughly, all samples underwent a 30-min incubation at 45 °C for protein-enzyme reaction before transferred to a 95 °C water bath for a 10-min enzyme inactivation (Shen, Hong, Singh, Koppel, & Li, 2022). After cooled down immediately in an ice bath, some samples were used in suspension state to test some following properties, while others were transferred to a −80 °C freezer for more than 24 h before freeze-dried for 5 days, to obtain lyophilised MTG-modified samples for other analysis.

2.3. Determination of physicochemical properties of MTG-modified proteins

2.3.1. Water holding capacity (WHC) and oil holding capacity (OHC)

For WHC analysis, 1 g of BRPI, PPI and their blends in different proportions: BRPI + PPI (8:2); BRPI + PPI (6:4); BRPI + PPI (4:6); BRPI + PPI (2:8) were transferred to a pre-weighed centrifuge tube respectively, followed by adding 10 mL of MTG aqueous solution at different concentrations (0.5 U/g protein and 1.0 U/g protein). Same steps were performed for control group, in which 10 mL of the deionised water (DW) was used in place of MTG solution. Then all samples underwent same procedures of incubation, inactivation and cooling down as mentioned in Section 2.2, followed by a centrifugation at 4000×*g* at 25 °C for 25 min.

For OHC analysis, all MTG-treated protein blends as well as control group obtained from above were freeze dried, and 10 mL of the canola oil was added, followed by 30-min standing in room temperature and same centrifugation as mentioned above. The residues were weighted, the dry weight of each 1 g protein isolate at the beginning was measured by using an infrared moisture analyser (Sartorius MA37, Germany), and the protein content of each isolate was obtained by the Kjeldahl method (AOAC, 2005). Both WHC and OHC can be calculated based on the following equation:

$$\mathrm{WHC} \Big/ \mathrm{OHC} = \frac{\text{Weight of residue (g)} - \text{Weight of dry sample (g)}}{\text{Weight of protein (g)}}$$

2.3.2. Solubility

As prepared according to the methods mentioned in Section 2.2, the MTG-treated sample solution in each group was obtained. Then another 90 mL of acetate buffer (10 mM) was added into the protein suspension to reach a concentration of 1% (w/v), followed by being kept at 4 °C overnight to allow full hydration.

Then 2 M HCl or 2 M NaOH was used to adjust protein suspension to pH 3.5–8, and protein samples at each pH were centrifuged at 8000×*g* for 15 min at 4 °C, to determine the soluble protein level in the supernatants based on the Bradford method (Kruger, 2009). Protein solubility was calculated as the percentage of the soluble protein content over the total protein content added in the dispersion.

2.3.3. Zeta potential

The protein samples obtained after overnight hydration as mentioned above were diluted with acetate buffer again to achieve 0.1% (w/v) concentration, followed by same pH adjustment to the values of 3.5–8. Then a Nanoparticle analyser (Horiba SZ–100, Retsch Technology, Germany) with a disposable electrophoresis cell was used immediately to measure the zeta potential value of all samples at different pH values by electrophoretic mobility measurements at 25 °C (Du, Reuhs, & Jones, 2016).

2.3.4. Gelling property

The gel point temperature and the gel strength of MTG-modified proteins were determined by rheological analysis, before which the least gelling concentration (LGC) was investigated first according to a previous method with slight modifications (Sun & Arntfield, 2010). Protein solutions (30 mL) were made at concentrations of 14–24% (w/w) for control BRPI + PPI (4:6) blend, which were dissolved in 10 mM acetate buffer (pH 7) and stirred for 2 h. Then 0.6 mL of each solution was transferred to a 2 mL microtube and heated at 90 °C for 30 min. After that, samples were placed in the ice bath for 2 h before inverting the tubes to see the samples' fluidity. The sample with the lowest concentration that did not fall or slip was considered to be the LGC.

For rheological measurements, a stress-controlled rheometer (Anton Paar, Graz, Austria) equipped with a PP 40 parallel plate geometry was used. The lyophilised control and MTG-modified BRPI + PPI blends obtained from Section 2.2 were dissolved in acetate buffer to achieve the desired LGC respectively, and stirred for 2 h before loading 1.3 mL onto the sample holder. The gap between the upper and lower plates was adjusted to 1 mm and the sample edges were covered mineral oil to prevent drying. Temperature ramps were performed first by heating the samples from 25 °C to 90 °C at the rate of 4 °C/min, holding the sample at 90 °C for 10 min and cooling to 4 °C at the same rate, with a constant shear strain of 1% and frequency of 0.1 Hz (Truong, Clare, Catignani, & Swaisgood, 2004). After maintaining at 4 °C for 15 min, frequency sweeps were conducted from 0.1 to 10 Hz at the same temperature.

2.4. Characterisation of protein profiles of MTG-modified proteins

Sodium dodecyl sulphate polyacrylamide gel electrophoresis (SDS-PAGE) was used to characterise the protein profiles before and after MTG treatments, under reducing and non-reducing conditions, respectively. For reducing condition, the combination of 900 μL of 4x Laemmli sample buffer (Bio-rad, USA) and 100 μL of 2-mercaptoethanol (Sigma-Aldrich, USA) was prepared freshly and served as sample treatment buffer (STB) (Zhao, Zhao, Phey, & Yang, 2019). Then 300 μL of protein suspension in each treatment group as prepared following the same procedures in Section 2.2 with desired dilution was mixed thoroughly with 100 μL of STB, followed by 5-min heating at 95 °C. After centrifugation (6000×*g*, 4 °C, 10 min), 10 μL of the protein supernatants was injected into the Mini-protean® TGX™ precast protein gel (Bio-Rad, USA) for electrophoresis. The proteins were fractionated at 120 V in a Bio-Rad Mini-Protean II cell (Bio-Rad, USA) containing Tris/Glycine/SDS running buffer (Bio-Rad, USA). The gel was taken out from the tank when the front band reached its bottom (around 1 h), followed by 1-h staining in InstantBlue® Coomassie protein stain (Abcam, USA) under mild shaking with no further destaining step. After rinsed several times in DW, the stained gels were analysed using Amersham Imager 600 (GE Healthcare Life Science, USA).

A series of molecular weight (MW) markers (2–250 kDa, prestained protein standards, Bio-Rad, USA) was run on the same gel for our protein band identification. The samples in non-reducing group underwent the same operating steps except that DW was used in STB preparation in place of 2-mercaptoethanol. To determine each polypeptide band's MW and intensity, ImageJ (version 1.53k) was used and the relative concentration of each identified polypeptide band in each treatment group can be quantified.

2.5. Determination of secondary structure of MTG-modified proteins

All lyophilised MTG-modified protein samples obtained from Section 2.2 were sent to an attenuated total reflectance-Fourier transform infrared (ATR-FTIR) spectrometer (PerkinElmer Inc., USA) for protein secondary structural characterisation. Spectrum of each sample within the range of 4000–650 cm^{-1} was recorded after 32 scans with a resolution of 4 cm^{-1}, in which the amide I region (1700–1600 cm^{-1}) underwent further deconvolution by OriginPro 9.0 software (OriginLab, Northampton, MA, USA), under the function of Gaussian curve fitting (Huang, Mao, Li, & Yang, 2021). The proportion of each secondary structure (e.g., α-helix, β-sheet, β-turn, and random coil) was calculated from the relative integrated areas of each component peak.

2.6. In vitro digestion of MTG-modified proteins

A three-phase model including oral, gastric and intestinal *in vitro* digestion was applied based on the protocol described in previous references (Brodkorb et al., 2019; Minekus et al., 2014). The electrolyte stock solutions used in each digestive stage were prepared according to the formula listed in Table S2, which introduced simulated salivary fluid (SSF), simulated gastric fluid (SGF), and simulated intestinal fluid (SIF) compositions in detail. Before digestion, all MTG-treated protein solutions obtained in Section 2.2 were warmed first at a 37 °C water bath.

In the simulated oral processing stage, 5 mL of electrolyte solution containing 4 mL of α-amylase SSF solution (enzyme activity in final digesta: 75 U/mL), 25 μL of $CaCl_2$ solution (0.3 M) and 0.975 mL of DW was mixed thoroughly, followed by pre-warmed to 37 °C before mixed with 5 mL of each protein samples, reaching a total volume of 10 mL in the final digesta, which was continually incubated at 37 °C in a shaking water bath with speed of 200 rpm for 2 min.

In the simulated gastric digestion stage, 10 mL of electrolyte solution containing 8 mL of pepsin SGF solution (enzyme activity in final digesta: 2000 U/mL), 5 μL of $CaCl_2$ solution (0.3 M) and 1.995 mL of DW + HCl (2 M, to adjust final digesta pH to 3.0) was prepared and warmed at 37 °C as well, followed by added into the oral phase products to obtain a total volume of 20 mL in the final digestion mixture, which was continually incubated at 37 °C in a shaking water bath with speed of 200 rpm for 2 h.

In the simulated intestinal digestion stage, 20 mL of electrolyte solution containing 16 mL of pancreatin SIF solution (enzyme activity in final digesta: 100 U/mL based on trypsin activity), 40 μL of $CaCl_2$ solution (0.3 M), 80 μL of amyloglucosidase and 3.88 mL of DW + NaOH (2 M, to adjust final digesta pH to 7.0) was prepared, and 0.1768 g of bile was added in it, requiring 30-min exhaustive mixing in a 37 °C shaking water bath for complete bile solubilisation. After that, the total liquid mixture was poured into the gastric phase products to obtain a total volume of 40 mL in the final digestive mixture, which was continually incubated at 37 °C in a shaking water bath with a speed of 200 rpm for 2 h. Then the samples were heated immediately in 95 °C water for 10 min to inactivate digestive enzymes and stop digestion reaction. The release of amino acids from each MTG-modified protein digest was analysed in the following sections.

2.7. NMR analysis

The digesta of each MTG-modified protein sample was centrifuged at 10000×*g* for 5 min at 4 °C, to discard the precipitates that cannot be digested by human digestive system. The supernatants were filtered through 0.22 μm membrane before freeze-dried for 5 days for NMR analysis. On the other hand, same amounts of all digestive enzymes and chemicals used during digestion were mixed with acetate buffer (no protein samples) and underwent the whole digestion phases, to obtain the NMR spectral signals of those digestive enzymes.

Each freeze-dried sample (35 mg) was mixed well with 1 mL of deuterated water (D_2O, 99.9%) containing 0.01% sodium 3-trimethylsilyl [2,2,3,3-d_4] propionate (TSP, Sigma-Aldrich, USA), followed by 10-min centrifugation at 4 °C under 12000×*g* speed (Zhao, Zhao, Wu, Lou, & Yang, 2019). Then 600 μL supernatants were pipetted into 5-mm (diameter) NMR tubes for following measurement.

^1H spectrum of each sample was obtained by a Bruker's Triple Resonance probe, which was set at 800 MHz to test sample under 25 °C (Bruker Avance Neo NMR Spectrometer, Rheinstetten, Germany). Standard NOESY setting (noesypr1d) was used to collect 1D spectra,

whose detailed parameter setting could be found in our previous study (Zhao et al., 2022). For spectra processing, the phase adjustment and baseline correction of each spectrum was conducted first by TopSpin 4.0.3 (Bruker). Several databases like Biological Magnetic Resonance Data Bank (http://www.bmrb.wisc.edu/) and Human Metabolome Database (http://www.hmdb.ca/) were used as references to identify amino acids from 1D ^{1}H spectra. Mestrenova (Mestreab Research SL, Santiago de Compostela, Spain) was used next to deal with peak normalisation, followed by binning data with equal width of 0.02 ppm.

The binned data were then processed by principal component analysis (PCA) in SIMCA software (version 14.0, Umetrics, Sweden) to show the separation of each data set and the responsible amino acids. Besides, the orthogonal projection to latent structure discriminant analysis (OPLS-DA) was performed to show intergroup metabolomic differences between control and MTG-treated group in each protein sample. To screen significant amino acids that were susceptible to MTG treatment, the scores of variable importance in projection (VIP) in each pairwise comparison were analysed (He, Zhao, Chen, Zhao, & Yang, 2021).

2.8. Statistical analysis

Each experiment was performed in duplicate independently, followed by duplicate sampling in each parallel test. The results were presented as mean values ± standard deviations. The Duncan's multiple range test and one-way analysis of variance (ANOVA, $P < 0.05$) were used to reveal statistically significant differences among different treatment groups, with a SPSS software (version 24; IBM Co., Armonk, NY, USA).

3. Results and discussion

3.1. MTG effects on protein physicochemical properties

3.1.1. WHC and OHC

Fig. 1 shows the impact of MTG concentration on WHC and OHC of BRPI and PPI. In control group with no MTG, increased WHC was achieved immediately when PPI was used to replace 20% BRPI. However, with the increasing proportion of PPI in the mixture, no more increase and even decrease in WHC was observed as compared to that in BRPI alone, which was probably related to higher solubility of pea protein in water in place of absorbing and holding the water (Shen & Li, 2021). It was worth noting that under MTG treatment, significant increase of WHC was observed in all BRPI + PPI blend from 6:4 ratio onwards, with 10.1%, 33.8%, 26.4% and 30.4% enhancement in BRPI + PPI blend of 6:4, 4:6, 2:8 and 0:10 after 0.5 U/g protein MTG treatment, respectively and 40.6%, 91.6%, 91.0% and 79.6% enhancement in BRPI + PPI blend of 6:4, 4:6, 2:8 and 0:10 after 1.0 U/g protein MTG treatment, respectively, as compared to that in control group with no MTG (Fig. 1A). Considering both brown rice protein and pea protein contained appreciable quantities of Glu, which could react with NH_4^+ to form Gln, and pea protein was rich in Lys (Jiang et al., 2017; Kalman, 2014), the originally small protein fragments in BRPI + PPI blend could be crosslinked into large lumpy proteins under MTG treatment due to sufficient substrate contained, forming continuous network structures to trap water.

On the contrary, MTG treatment significantly decreased OHC of BRPI and PPI blend, with 12.5%, 31.1%, 39.3% and 10.1% reduction in BRPI + PPI blend of 8:2, 6:4, 4:6, and 2:8 after 1.0 U/g protein MTG treatment, respectively, as compared to that in control group with no MTG (Fig. 1B). OHC is associated with the number of exposed hydrophobic amino acid residues located on the protein surface, as well as the level of hydrophobic amino acids (Shen, Tang, & Li, 2021). The results shown in our study suggested that the crosslinking occurring between Lys and Gln residues might not cause significant alteration of the exposed hydrophobic amino acids in pea protein alone, and when blended with BRPI, even less hydrophobic regions were exposed after MTG treatments.

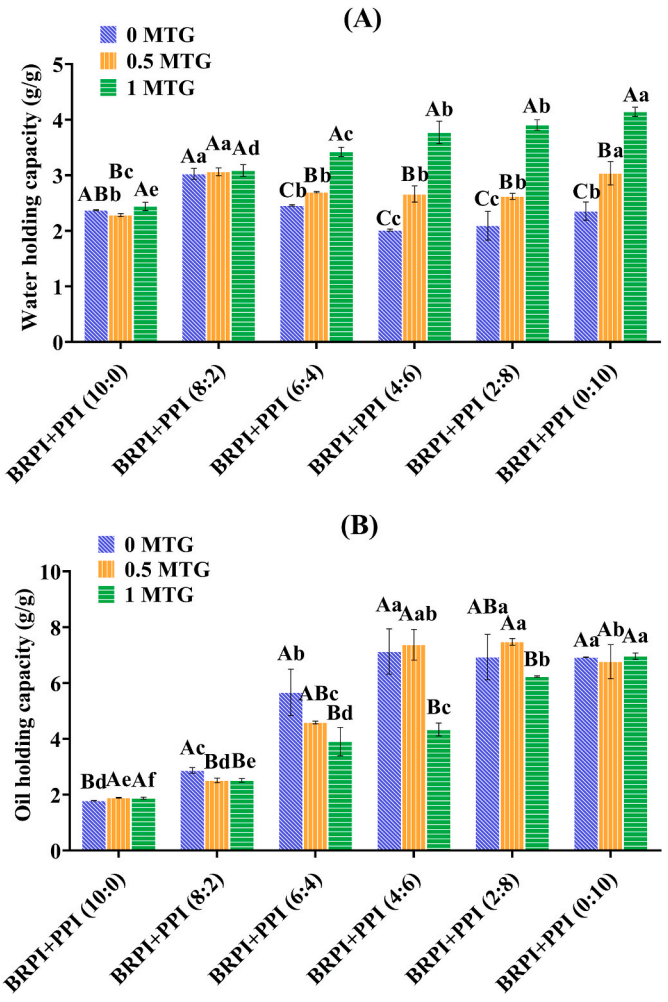

Fig. 1. Effect of MTG concentration on WHC (A) and OHC (B) of BRPI and PPI blend. Data are presented as mean values ± standard deviation. Mean values within the same mix proportion by different treatments with different capital letters are significantly different; mean values for the same treatments in different mix proportion with different lowercase letters are significantly different ($P < 0.05$). WHC: Water holding capacity; OHC: Oil holding capacity.

Similar results were also found in MTG-treated casein, whey protein, and soybean globulin in previous studies (Liu & Damodaran, 1999; Yildirim, Hettiarachchy, & Kalapathy, 1996). Considering the most significant differences of WHC and OHC between untreated and MTG-treated samples both occurred in the group of BRPI + PPI (4:6), this blend was chosen as a mixed example for following tests.

3.1.2. Solubility

The influences of MTG concentration on solubility of BRPI, PPI and their blends are shown in the left side of Fig. 2. Protein solubility in aqueous systems varies with the pH value (Cao, Wen, Li, & Gu, 2009). Lower solubility was observed within the range of pH 4–5 for both brown rice protein and pea protein, indicating their isoelectric points were both within this range. The extreme low solubility (<1%) of BRPI throughout the whole pH range might be attributed to the native structure of its main component, glutelin (~80% in total proteins), which was insoluble in water due to its high MW structures and only soluble in acid (pH < 3) or alkali (pH > 10) when protein structural conformations changed (Amagliani, O'Regan, Kelly, & O'Mahony, 2017). By contrast, the protein samples containing PPI displayed higher water solubility in the same pH range, as shown in Fig. 2BC. This might be due to pea protein's predominant compositions of globulins (ca. 55–80%) and albumins (ca. 15–25%), which generally display low

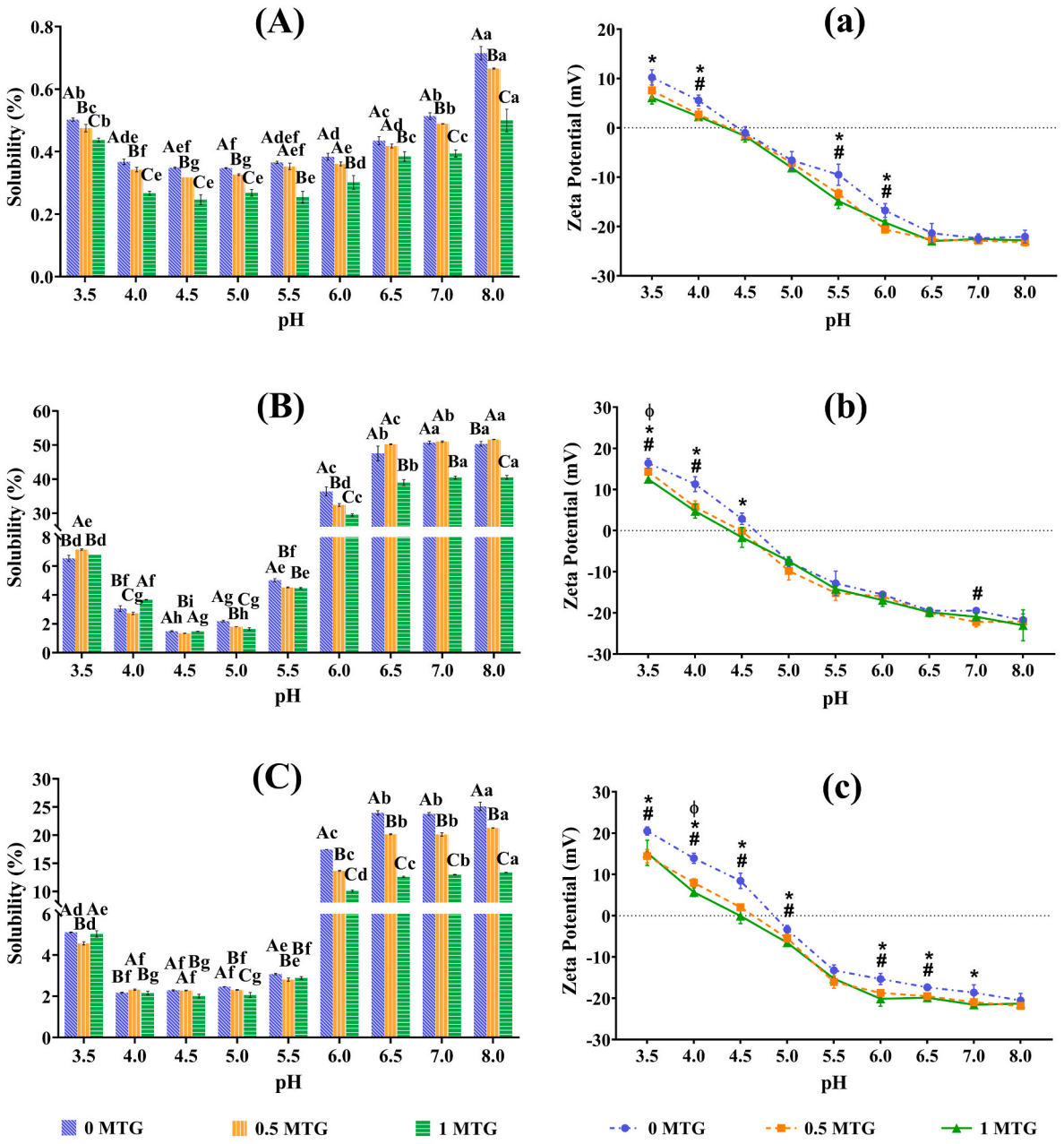

Fig. 2. Effect of MTG concentration on solubility and zeta potential of BRPI (A), PPI (B) and BRPI + PPI (4:6) (C). Data are presented as mean values ± standard deviation. For solubility, mean values within the same pH by different treatments with different capital letters are significantly different; mean values for the same treatments in different pH with different lowercase letters are significantly different ($P < 0.05$). For zeta potential, the marks #, * or ϕ indicate statistically significant differences ($P < 0.05$) between 0 MTG and 0.5 MTG, 0 MTG and 1 MTG, and 0.5 MTG and 1 MTG, respectively, at each pH.

surface hydrophobicity and good protein–water interactions (Djoullah, Djemaoune, Husson, & Saurel, 2015).

After MTG treatments, most protein samples' solubility gradually decreased with the increase of MTG concentration at the same pH, which could partly be attributed to the formation of insoluble macromolecular polymers as protein underwent aggregation and intramolecular or intermolecular crosslinking under MTG treatments (Li et al., 2022). This modification can change the gelation property of proteins, expanding their uses in various food applications. However, on the other hand, the compact structure of some proteins such as globulins in PPI might limit MTG's access to Gln and Lys residues to a certain extent. Thus, protein solubility could not be directly correlated with the degree of crosslinking (DeJong & Koppelman, 2002), which was more pronounced in the protein samples containing PPI at low pH levels (<5.5) in our study. Considering the variations in protein's net charge could also be responsible for the protein solubility changes, the pH-dependence results of zeta potentials of our protein blends were further investigated in the following section.

3.1.3. Zeta potential

The right side of Fig. 2 shows the effects of MTG concentration on the net charge of BRPI, PPI and their blends indicated by zeta-potential. The isoelectric point (pI) is known as the pH value at which protein carries no effective net charge (0 mV), which is an important factor in determining protein aggregation, particle sizing and stability (Malhotra & Coupland, 2004). The pI values of our control BRPI and PPI samples were around 4.4 and 4.6, respectively, indicating BRPI might contain higher level of acidic amino acids on the surface of protein than PPI but

not infallible, as the protein folding could also play a part (Solovyev, Tarnovskaya, Chernova, Shataeva, & Skorik, 2015). With the pH decreasing from 8.0 to 3.5, zeta potentials of all protein samples gradually increased from a negative value to a positive value, which could be due to the gradual variations of the protonation and deprotonation states of protein's carboxyl groups and amino groups respectively along with the changes of surrounding environmental pH (Tang & Sun, 2011). On the other hand, the zeta potential of BRPI alone varied from +10 mV to −20 mV along with the pH change from 3.5 to 8, while other groups containing PPI had a wider scope of +20 mV to −20 mV within the same pH range. This difference may be due to the less amount of Lys available in cereal proteins than in legume proteins, as at low pH, basic amino acids such as Lys can accept proton and be positively charged, determining the net charge of the total protein systems (Gorissen et al., 2018).

MTG-catalysed crosslinking could make the number of positive charges in proteins reduced, as the acyl-transfer reactions happening between Gln and Lys residues could lead to an amino group loss (Zhang et al., 2022). This can explain why decreased zeta potentials of MTG-modified BRPI and PPI were observed at most pH values in our study, as well as lower pI of all kinds of protein samples after MTG treatment as shown in Fig. 2. Moreover, the significant differences of zeta potential between the control group and MTG-treated groups appeared mainly in the BRPI and PPI blend, as shown in Fig. 2c, indicating that there might be synergistic effects of MTG on the combined plant protein than on each alone. A previous study demonstrated that MTG could play a role in rearranging the distribution of surface amino acids, so the decreased zeta potentials shown in our protein samples might also be related to the increased amount of negatively charged surface amino acids after MTG treatments, contributing to a more negative net charge (Wang, Zhong, & Hu, 2013). Furthermore, some researchers found that the contents of free SH groups and disulfide bonds in proteins could also be influenced by MTG-induced crosslink, which might contribute to the reduction of positive surface charges to some extent (Tang, Wu, Chen, & Yang, 2006; Zhang et al., 2016).

3.1.4. Gelling property

The vicilin to legumin (V/L) ratio of our PPI used in this study was around 3.43 under non-reducing condition and 1.87 under reducing condition (data not shown), based on the following SDS-PAGE results which will be discussed in Section 3.2. In a previous study, Barac et al. (2010) used the same way to investigate pea protein compositions from six genotypes and found their V/L ratios were mostly concentrated in the range of 1.28–2.09 under non-reducing condition whereas 1.06 to 1.49 under reducing condition. Therefore, our PPI with higher ratio of V/L could be more suitable for protein gelation (Sun & Arntfield, 2010). In this part, we used BRPI + PPI blend as a representative to show the impact of MTG on their gelling property changes. The LGC is an index which could evaluate the gelation capacity of the protein (Zhu, Lin, Ramaswamy, Yu, & Zhang, 2017). In our study, the LGC of control BRPI + PPI (4:6) blend was 20%, as shown in Fig. S1, so we prepared protein suspension with this concentration to do rheological analysis.

Fig. S2 shows the rheological properties of BPRI + PPI blend after 1 U/g MTG treatment, which demonstrated distinguished differences compared to those of control group. We adopted viscosity-based method to measure the gelation temperature of our samples, as the crossover point of storage modulus (G′) and loss modulus (G") of our samples was not observed in our preliminary trials. By monitoring the viscosity, which would increase suddenly near the gelation temperature, we can see the gel point temperature of BRPI + PPI treated by 1 U/g MTG was decreased significantly, from 84 °C to 45 °C as shown in Fig. S2 (A). This phenomenon indicated that MTG-catalysed samples needed less heat to form a gel which was already formed enzymatically to some extent (Wilcox & Swaisgood, 2002). During cooling process, the G′ and G" values of control group increased steadily, indicating some cross-linking like hydrophobic interactions and hydrogen bonds might continue, although at a slower rate, contributing to the formation and rearrangement of the network structure (Sun & Arntfield, 2010). On the other hand, an obvious increase in the gel strength of MTG-catalysed sample with drastically higher storage modulus was clearly shown in Fig. S2 (B), demonstrating the reinforcement of the gel structure persisted more starkly as it cooled after MTG treatment. Moreover, the tan δ values of MTG-treated sample were lower than those of control group throughout the cooling process, indicating an improvement of the gel elasticity in MTG-treated BRPI + PPI blend. Upon cooling to 4 °C, subsequent frequency sweep test was conducted, to provide valuable insights into the gel's final properties. As shown in Fig. S2 (C), it can be inferred that BRPI + PPI blend without MTG treatment formed a weak gel because of its lower G′ values and higher tan δ values, whereas more solid-like behaviour with better three-dimensional structures (lower tan δ values) and increased network strength (higher G′ values) was shown in MTG-catalysed group. Our results were consistent with previous studies that MTG-induced crosslinks could result in stronger and more elastic gels with lower gel point temperature, enhancing existing functional properties to facilitate various food protein applications (Herz, Schäfer, Terjung, Gibis, & Weiss, 2021; Wilcox, Clare, Valentine, & Swaisgood, 2002).

3.2. MTG effects on protein profiles

The changes of protein profile of MTG-modified BRPI, PPI and their blend were characterised by using SDS-PAGE, under both non-reducing and reducing conditions. In this part, we increased the concentration of MTG to 10 U/g protein to magnify its effects on protein profile to have a better understanding of the behaviour of each fraction constituting brown rice and pea proteins under MTG treatments.

As shown in Fig. 3A, the mostly contained polypeptides in BRPI with a MW around 50 kDa under non-reducing condition is recognised as glutelin, which was composed of two subunits linked by disulfide bonds, i.e., the acidic glutelin subunits (30 kDa) and the basic glutelin subunits (20 kDa). The glutelin polypeptide band intensities increased significantly under reducing condition, which is a phenomenon consistent with the findings reported previously (Kupkanchanakul, Kadowaki, Kubota, & Naivikul, 2018). However, the number and intensities of the protein bands for all MTG-treated BRPI were similar under both non-reducing and reducing conditions, respectively, indicating that the two most abundant proteins in brown rice, i.e., glutelins and prolamins, might not provide desirable availability and accessibility of substrates to MTG due to their hydrophobic properties, demonstrating no significant MTG effects from SDS-PAGE direct visualization (Netrprachit, Ogawa, & Suwannaporn, 2019).

Unlike BRPI, globulins and albumins are the two most abundant proteins in PPI, which have been considered attractive candidates for MTG crosslinking due to their salt-soluble and water-soluble properties as well as relatively high Gln and Lys concentrations (Casey, 1982). Most of the bands observed in our study belonged to globulin fraction, which was composed of legumins (acidic Legumin α (Lα) 37 kDa and basic Legumin β (Lβ) 20 kDa), vicilins (48, 27–32, 16, and 13 kDa) and convicilin (71 kDa). On the other hand, the albumin fraction included lipoxygenase (89 kDa), pea albumin PA2 (26 kDa) and PA1 (8–11 kDa), which were also exhibited in our SDS-PAGE profiles. Legumin has been described as a hexamer with acidic and basic polypeptides connected by disulfide bonds, that's why higher intensities of their bands (Lα 37 kDa and Lβ 20 kDa) were observed under reducing condition (Fig. 3B). However, previous studies found that most of the Lα subunits were located on the protein surface while Lβ subunits constituted the inner hydrophobic core (Moreno et al., 2020), which might explain why Lα bands grew fainter with the increasing concentration of MTG while Lβ remained mostly intact in our SDS-PAGE result, owing to the different location of the reactive residues. In general, fewer and fainter bands were shown in the PPI treated by MTG at concentrations of 4 U/g protein and above in our study, under both non-reducing and reducing conditions. These results agreed with the previous findings that some pea

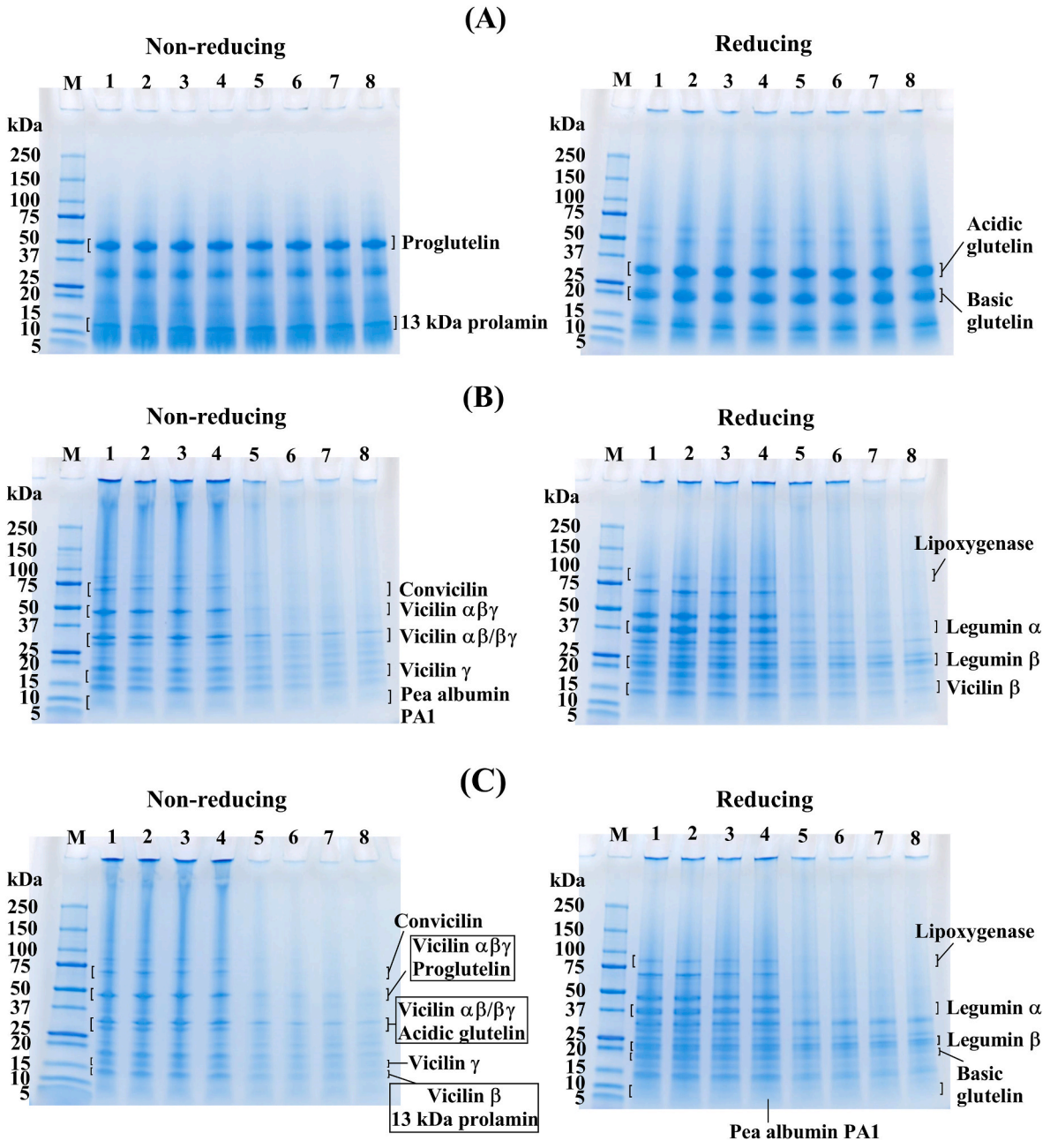

Fig. 3. SDS-PAGE profiles of untreated and MTG-treated BRPI (A), PPI (B) and BRPI + PPI (4:6) (C) under non-reducing and reducing conditions. M: molecular weight marker; 1: control group (no MTG); 2–8: MTG at concentration of 0.5, 1, 2, 4, 6, 8 and 10 U/g protein, respectively.

globulin bands (e.g., convicilin 71 kDa, vicilins 55, 50 and 35 kDa, Lα 40 kDa) could completely disappear when a high concentration of MTG was applied, as the formed large polypeptides were hard to be extracted to enter the running gel (Djoullah et al., 2015). For albumins, only lipoxygenase (89 kDa) bands gradually faded away as the MTG concentration increased, indicating the PA1 and PA2 sections were relatively poor substrates to MTG due to their compact structures that limited MTG's access to Gln and Lys reactive residues (Bhatty, 1982).

When BRPI and PPI were blended, its protein profile pattern looked similar to that of PPI alone, and some bands of BRPI + PPI blend would be the sum of BRPI and PPI of the same MW as shown in Fig. 3C. To better understand whether MTG had a synergistic or other effect on certain protein band(s) in the BRPI + PPI blend than in each alone, the relative concentration of each identified polypeptide band in these three protein groups was quantified, as shown in Fig. S3. The control group (no MTG added) bands were used as references with scores set at 1, and all MTG-treated protein bands' intensities were compared to the control bands. A lower score below 1 indicates that the protein identified in a particular band is more susceptible to MTG treatment. Vice versa, a higher score above 1 indicates the protein is less susceptible to MTG treatment.

The different variation patterns of the normalised intensity ratio of each band between non-reducing and reducing conditions could be attributed to the formation of MTG-induced disulfide bonds to a certain extent (Tang et al., 2006). For example, an evident decrease in the intensity of PPI's lipoxygenase bands was observed after MTG treatments in all concentrations under non-reducing condition, whereas under reducing condition, significant decrease only happened at MTG concentrations of 4.0 U/g protein and above (Fig. S3 (B)). This indicates that at low concentrations of MTG treatments, SH groups or sulfur-containing amino acids of lipoxygenase might be more exposed to the aggregates' surface, facilitating intermolecular disulfide bond

formation, which could make polypeptides hard to be extracted to enter running gel (Zhang et al., 2016). Whereas in the presence of reducing agent, the rupture of disulfide bonds facilitated the extraction of proteins from large polypeptides that retain the band's intensity from decreasing (Marco, Pérez, Ribotta, & Rosell, 2007).

With the concentration of MTG increased, all protein fractions of BRPI showed generally similar band intensity to that of the control group under both reducing and non-reducing conditions, except the 10 U/g MTG-treated BRPI sample, in which some changes in the intensity of bands in all BRPI fractions were observed under non-reducing condition

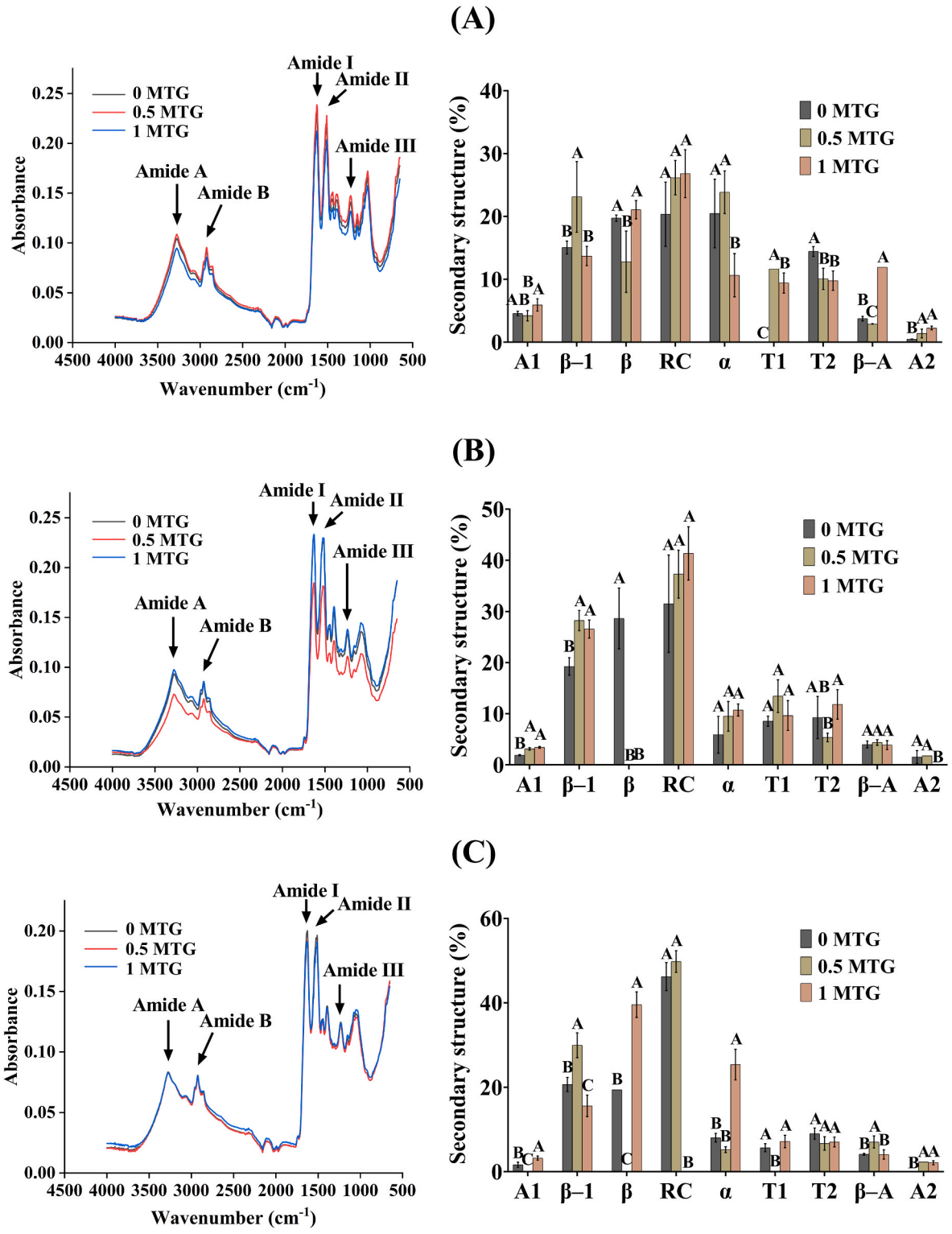

Fig. 4. FTIR spectra and the percentage of each secondary structure of BRPI (A), PPI (B) and BRPI + PPI (4:6) (C) after different MTG treatments. Note: A1 (1610–1615 cm^{-1}): intermolecular protein aggregates or the absorption of amino acid side-chains; β–1 (1618–1630 cm^{-1}): intermolecular β-sheets; β (1630–1638 cm^{-1}): native β-sheets; RC (1640–1648 cm^{-1}): random coils; α (1650–1660 cm^{-1}): α-helixes; T1 (1660–1670 cm^{-1}): β-turn conformations; T2 (1670–1680 cm^{-1}): β-turn conformations; β–A (1680–1688 cm^{-1}): antiparallel β-sheets; A2 (1690–1695 cm^{-1}): protein aggregates.

(Fig. S3 (A)), while not visible from SDS-PAGE images. On the other hand, the normalised intensity ratio of protein bands in PPI and BRPI + PPI blend showed similar variation patterns in all protein fractions under both conditions, except for vicilin αβ, whose bands disappeared more apparently in PPI alone after MTG treatments than in BRPI + PPI blend under reducing condition (Fig. S3 (B), (C)). This might be due to the interaction of pea and brown rice protein, which might reduce MTG activity at various points of the vicilin αβ chain, making it unable to aggregate with no formation of new protein polymers (Marco et al., 2007). The presence of PPI, in turn, could also induce a different aggregation behaviour of BRPI in part under MTG treatments, because different band intensity ratios of BRPI fractions are shown between Fig. S3 (A) and (C), revealing the protein-protein interactions within the mixed systems at the molecular or supramolecular level.

3.3. MTG effects on protein secondary structures

FTIR analysis was conducted to further investigate the conformational variations of BRPI and PPI induced by MTG, as well as verifying their molecular interactions in the blend systems. The left side of Fig. 4 shows the spectra of BRPI, PPI and their blend after MTG treatments in the region of 4000–650 cm^{-1}. There was neither pronounced shifts in peak positions nor band appearing/disappearing in all spectra, implying that the addition of MTG in the selected protein systems might have insufficient effect on their skeletal conformations. Five major amide bands (i.e., amide A (3500–3200 cm^{-1}), amide B (3000–2800 cm^{-1}), amide I (1700–1600 cm^{-1}), amide II (1580–1400 cm^{-1}), amide III (1350–1200 cm^{-1})) were displayed among all the groups, with main peaks located in amide I and amide II regions in our protein samples, a phenomenon similar to other plant proteins such as chickpea and soy protein isolates demonstrated by Withana-Gamage, Wanasundara, Pietrasik, and Shand (2011). Considering the complex coupling vibrations of amide II peak, which mostly resulted from N–H bending and C–N stretching, use of the amide II region is not fit to provide complementary information for protein secondary structure characterisation (Carbonaro, Maselli, Dore, & Nucara, 2008). By contrast, the amide I band derived mainly from C═O stretching vibrations is commonly used for revealing protein secondary structures due to its stronger peak intensity, by determining the corresponding peak intensities quantitatively (Yu, 2005).

Therefore, to further understand the conformational differences of proteins in different MTG-treated groups, the amide I regions of all protein samples underwent Fourier self-deconvolution for separating the overlapped component peaks and enhancing the resolution of each peak component (Sow & Yang, 2015). Specifically, nine band ranges corresponding to protein secondary structures were identified as follows: 1610–1615 cm^{-1} (A1): intermolecular protein aggregates or the absorption of amino acid side-chains; 1618–1630 cm^{-1} (β–1): intermolecular β-sheets; 1630–1638 cm^{-1} (β): native β-sheets; 1640–1648 cm^{-1} (RC): random coils; 1650–1660 cm^{-1} (α): α-helixes; 1660–1670 cm^{-1} (T1): β-turn conformations; 1670–1680 cm^{-1} (T2): β-turn conformations; 1680–1688 cm^{-1} (β–A): antiparallel β-sheets; 1690–1695 cm^{-1} (A2): protein aggregates (Carbonaro, Maselli, & Nucara, 2012). An example of the curve fitting in deconvoluted FTIR spectra of amide I is shown in Fig. S4. The percentage of each secondary structure on the BRPI, PPI and their blend after different MTG treatments was calculated and shown in the right side of Fig. 4.

For BRPI alone, the relative spectral weight of the β–1 band was significantly increased after 0.5 U/g MTG treatment (from 15 to 23%), accompanied by a decrease in β (−7%) and β–A (−0.8%) band. When the MTG concentration increased to 1 U/g, an evident reduction of α-helix band was observed as compared to the control group (from 20 to 10%). Most consistent modifications consisted in the increase of the T1 and A2 band and in the decrease of T2 band in all MTG-treated groups (Fig. 4A). For PPI alone, a disappearance of the β band was shown in all MTG-treated samples, paralleled by an increase in β–1 and A1 band (Fig. 4B). Previous studies demonstrated that thermal treatment could induce the formation of intermolecular β-sheet aggregates (β–1 band) followed by the loss of β-sheet structures in various legume species (Carbonaro et al., 2012; Mills et al., 2003). Considering all protein samples in our study experienced the same heating treatment in Section 2.2 for enzyme inactivation, the formation of protein aggregates with more intermolecular β-sheet aggregates could be attributed to the MTG enzymatic crosslinking (Qin et al., 2016). Moreover, the increase of the relative spectral weights of the A2 band in BRPI and the A1 band in PPI after MTG treatments might be related to the higher accessibility of amino acid side chains in the MTG-treated proteins, which could be served as markers for intermolecular protein complexes as well (Carbonaro et al., 2012).

Although the RC relative spectral weight in BRPI and PPI alone remained almost stable over different MTG treatments, when they were blended, lower level of RC paralleled by an increase in both β-sheet structures and α-helix band were observed in the 1.0 U/g MTG-treated BRPI + PPI blend as compared to those in the control group (Fig. 4C), verifying again that the protein-protein interactions within the mixed systems might enhance the function of MTG in the structural modification, facilitating the network formation of more ordered and compact structure and improving the thermal stability and the strength of protein gels (Lu, Lee, & Yang, 2022). The 1 U/g MTG-induced BRPI + PPI aggregates containing β-sheet as its main secondary structural component might display some amyloid-like features in a way, similar findings also stated in previous studies (Chan, Pinotsi, Gabriele, Schierle, & Kaminski, 2014; Villar-Piqué et al., 2010), which made the changes in the physicochemical properties and SDS-PAGE images of our protein blend reasonable as shown above.

3.4. Amino acid profiles after in vitro digestion

The amino acid bioavailability of MTG-treated protein samples is one important indicator of their nutritional values, however, studies on how the MTG-induced crosslinking affects the amino acid release and the digestive performance of plant-based proteins have yet to be fully engaged (Jiménez-Munoz, Tavares, & Corredig, 2021). Our study represents the first attempt to use NMR-based metabolomics to elucidate the digestive characteristics of MTG-modified supramolecular structures during *in vitro* digestion.

The corresponding ^{1}H NMR spectra of metabolite extracts from MTG-treated BRPI, PPI and their blend after *in vitro* digestion are shown in Fig. 5. Based on signals from 0.5 to 9.5 ppm, there were totally 22 amino acids identified, and the detailed chemical shift assignments of each amino acid are listed in Table 1. In general, the spectra showed a high degree of similarity in amino acid varieties in different protein sources, with most of them concentrated in the range of 1.0–4.0 ppm. On the other hand, some amino acids displayed different signal intensities from different protein sources. For example, the peaks of Ala and Tyr were more significant in BRPI's digesta as compared to those in PPI's digesta, which agreed with previous studies stating their amino acid contents (Gorissen et al., 2018). Moreover, some amino acid levels showed a downward trend after MTG treatments, such as Tyr and Phe, whose peaks became lower in PPI as the concentration of MTG went up. Monogioudi et al. (2011) found that the formation of high molecular polymers induced by MTG treatment could affect the digestive enzymes' ability to access the reactive sites of proteins, accompanied by a decreased digestibility of the proteins. Therefore, to identify which amino acids' bioavailability in BRPI and PPI were most affected by MTG after *in vitro* digestion, subsequent PCA and OPLS-DA analyses were conducted.

3.5. Principal components analysis

PCA was conducted to show the overall amino acid discrimination in different MTG-treated protein digesta, by using the method of

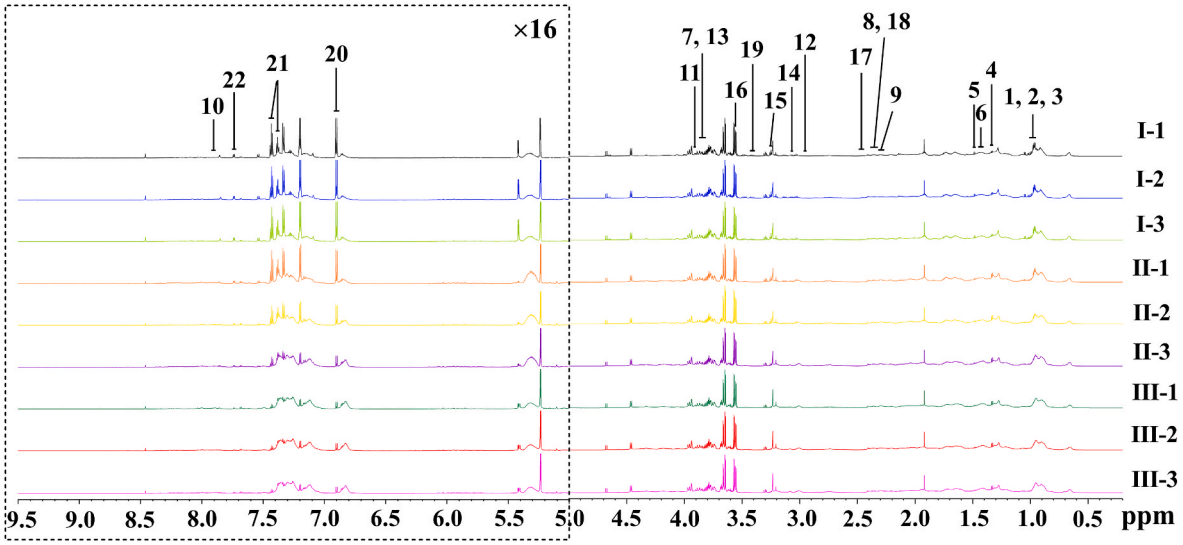

Fig. 5. Representative ^{1}H NMR spectra of metabolite extracts from MTG-treated BRPI, PPI and their blend after *in vitro* digestion. Note: I-1: BRPI without MTG treatment; I-2: BRPI with 0.5 U/g MTG treatment; I-3: BRPI with 1 U/g MTG treatment; II-1: PPI without MTG treatment; II-2: PPI with 0.5 U/g MTG treatment; II-3: PPI with 1 U/g MTG treatment; III-1: BRPI + PPI (4:6) without MTG treatment; III-2: BRPI + PPI (4:6) with 0.5 U/g MTG treatment; III-3: BRPI + PPI (4:6) with 1 U/g MTG treatment. Metabolites keys to the numbers are the same as Table 1.

Table 1
Amino acids identified in control and MTG-treated BRPI, PPI and their blend after *in vitro* digestion.

No.	Amino acid	δ^{1} H (ppm) and multiplicity[a]
1	Isoleucine	3.66 (d), 1.95 (m), 1.48 (m), 1.00 (d), 0.94 (t)
2	Leucine	3.74 (m), 1.73 (m), 1.71 (m), 0.97 (t), 0.94 (t)
3	Valine	3.60 (d), 2.26 (m), 1.04 (d), 0.99 (d)
4	Threonine	3.61 (d), 4.25 (m), 1.33 (d)
5	Alanine	3.76 (q), 1.48 (d)
6	Lysine	3.74 (t), 1.91 (m), 1.45 (m), 1.73 (m), 3.03 (t)
7	Methionine	3.85 (dd), 2.13 (m), 2.65 (t), 2.14 (m)
8	Glutamic acid	3.74 (dd), 2.14 (m), 2.36 (m)
9	γ-aminobutyric acid	2.28 (t), 1.91 (m), 3.03 (t)
10	Histidine	3.13 (dd), 3.23 (dd), 4.00 (dd), 7.09 (d), 7.90 (d)
11	Aspartic acid	3.90 (m), 2.86 (m), 2.65 (m)
12	Asparagine	4.00 (dd), 2.94 (m), 2.85 (m)
13	Serine	3.94 (m), 3.83 (t)
14	Cysteine	3.94 (dd), 3.06 (m)
15	Arginine	3.76 (t), 1.91 (m), 1.71 (m), 3.25 (t)
16	Glycine	3.57 (s)
17	Glutamine	3.76 (t), 2.12 (m), 2.45 (m)
18	Proline	3.30 (d), 2.01 (m), 2.34 (m), 4.07 (m)
19	Cystine	3.21 (dd), 3.40 (dd), 4.11 (dd)
20	Tyrosine	3.93 (dd), 3.05 (dd), 7.19 (d), 6.90 (m)
21	Phenylalanine	3.96 (dd), 3.23 (m), 7.33 (d), 7.43 (t), 7.38 (m)
22	Tryptophan	3.29 (dd), 3.47 (dd), 4.06 (dd), 7.19 (m), 7.27 (m), 7.33 (d), 7.53 (d), 7.73 (d)

[a] Multiplicity: s, singlet; d, doublet; t, triplet; q, quartet; dd, doublet of doublets; m, multiplet.

separation of variables from high throughput profiles (Zhao et al., 2022). In this study, the first three principal components (PCs) explained 91.4%, 93.3% and 88.0% of the total variance in BRPI's, PPI's and their blend's digesta respectively, accompanied by their Q^2 values all over 0.64 (>0.5), indicating that the model had a good interpretability and satisfying predictability (Fig. 6A1-C1). The samples from different MTG treatment groups were separated into 3 clusters and located at the different sides of three PCs, according to the score plot shown in Fig. 6A2-C2. Moreover, Table S3 and Table S4 display each PC's score plot variables and respective squared cosine values for each group, respectively. As can be seen, group I-1, I-2, I-3, II-1 and II-3 were affected mainly by PC1 while group II-2, III-1, III-2 and III-3 were characterised more by PC2 and PC3, respectively, indicating that differences of amino acid release caused by MTG were more significant in the protein samples containing PPI.

Moreover, the loading plot in Fig. 6A3–C3 shows the discriminative amino acids that contributed to the separated variables mentioned above. Most amino acids in BRPI's digesta were located at the positive side of PC1 and PC3 and the negative side of PC2, but were influenced more by PC1, as shown in Table S5 and Table S6. When combined with PPI, most amino acids released (e.g., GABA, Pro, Asn, Arg, Met, Trp) after *in vitro* digestion were located at the negative side of PC1 and the positive side of PC2 and PC3, with half of them more strongly correlated with PC3. By comparing the squared cosine values among the score variables and the loading observations, we found Leu, Val, Gln, Asn, Arg, Cys-Cys, Met, Tyr, Phe and Trp might contribute more to group separation of BRPI's digesta, while the group characterisation of PPI's digesta after different MTG treatments might be closely related to Leu, Val, Thr, Lys, Ala, Pro, Gln, Asn, Cys, Asp, Tyr, Phe, Trp and His. Considering PCA analysis just provided an overview of amino acid profiles of digested protein isolates after different MTG treatments, the protein-specific digestive responses to MTG crosslinking needed to be investigated further. Therefore, the pairwise amino acid variations of each protein sample responsible for the class separation were studied by using OPLS-DA models.

3.6. Comparison of amino acid release within pairwise groups

OPLS-DA was constructed between the control group and 1.0 U/g MTG treatment group respectively in BRPI, PPI and their blend. The score plots of three OPLS-DA models with all $R^2X > 0.886$ and $Q^2 > 0.982$ (good model fitness with high predictability, data not shown) showed significant intergroup separations in all protein samples, indicating differences in amino acid release occurred to all protein isolates after treated by 1.0 U/g MTG (upper-left corner of Fig. 7A–C). From the coefficient loading S-line plots, the main amino acids that caused pairwise differentiation can be identified, with the upward peaks showing a higher level of specific amino acid detected from the 1.0 U/g MTG treatment group and the downward ones indicating opposite trends (right side of Fig. 7A–C). The transition of peak colour from blue to red corresponded to the increase in the absolute value of correlation coefficient from 0 to 1, indicating that resonance became progressively more

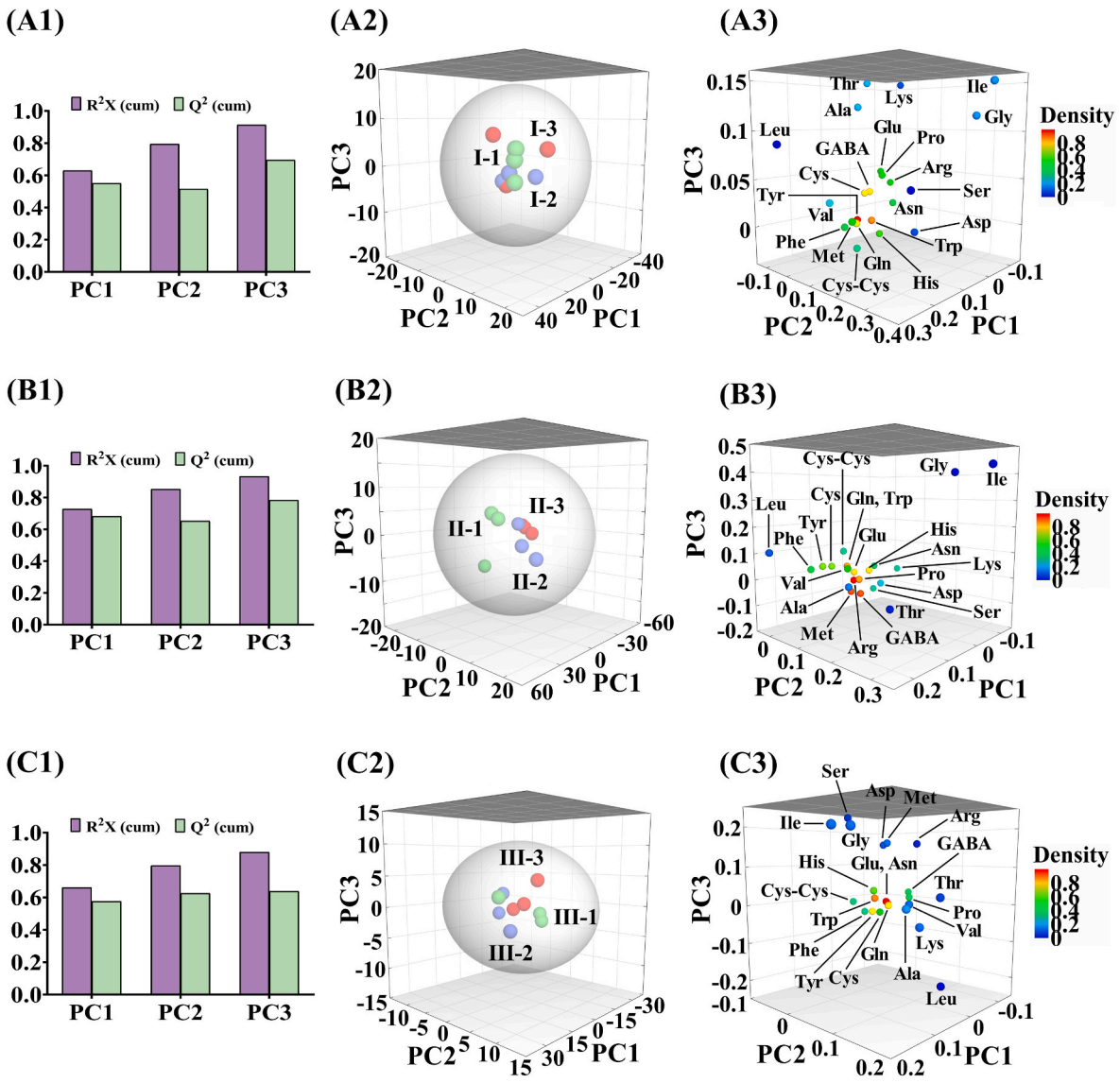

Fig. 6. Principal component analysis (PCA) for the metabolite profile of MTG-treated BRPI, PPI and their blend after *in vitro* digestion. A1–C1: The principal components explaining variances used in PCA; A2–C2: PCA score plot; A3–C3: PCA loading plot. Note: I-1: BRPI without MTG treatment; I-2: BRPI with 0.5 U/g MTG treatment; I-3: BRPI with 1 U/g MTG treatment; II-1: PPI without MTG treatment; II-2: PPI with 0.5 U/g MTG treatment; II-3: PPI with 1 U/g MTG treatment; III-1: BRPI + PPI (4:6) without MTG treatment; III-2: BRPI + PPI (4:6) with 0.5 U/g MTG treatment; III-3: BRPI + PPI (4:6) with 1 U/g MTG treatment.

important for distinguishing the metabolite profiles of pairwise groups (Zhao, Zhao, Wu, et al., 2019). The coefficient plot located at the lower-left corner of Fig. 7A–C demonstrates the MTG-induced increase (coefficient >0) or decrease (coefficient <0) in content of the 22 identified amino acids in each protein sample, which were regarded as statistically significant for contributing to the group distinction if their VIP values were more than 1 (Wu, Zhao, Lai, & Yang, 2021).

As shown in the loading S-line and the corresponding coefficient plot, the contents of most non-polar amino acids such as Leu, Trp, Phe and Val in all MTG-treated protein isolates were lower than those in control group after digestion, a similar result consistent with a previous study in which the MTG-treated surimi gels released less hydrophobic amino acids after digestion (Fang, Xiong, Hu, Yin, & You, 2019). It has been reported that MTG could affect the hydrolysis efficiency of pepsin and pancreatin, leading to different degree of protein degradation in the digestive system (Glusac, Isaschar-Ovdat, & Fishman, 2020). Therefore, the peptides containing hydrophobic amino acid residues in our MTG-treated BRPI and PPI might not be cleaved preferentially throughout the whole gastrointestinal digestion, maintaining their ordered structures in the final digests. On the other hand, considering the aromatic amino acids are perceived to be contributing factors in insulin resistance (Wang et al., 2021), the lower bioaccessibility of Phe and Trp in our MTG-treated plant proteins might make them have the potential to be incorporated into foods for individuals having diabetic complications.

It has been believed that the ε-(γ-Glu)-Lys (G-L) bonds formed by MTG exhibit strong resistance to pepsin. However, in the intestinal digestion stage, these isopeptide bonds could be hydrolysed under various actions of the proteases and peptidases (Fang et al., 2019; Lerner & Matthias, 2019). Hence, the increased level of Lys observed in our BRPI and PPI alone indicated that the networks formed by MTG cross-linking might be efficiently broken down at the end of digestion, demonstrating higher digestibility in MTG-treated proteins as compared to their uncrosslinked counterparts, which might be hydrolysed quickly at the beginning in gastric digestion but not be completely cleaved in the anaphase of intestinal digestion with a relatively flat release profile (Fang et al., 2019; He, Hu, Woo, Xiong, & Zhao, 2021). On the other hand, previous studies found Gln could be transformed to Glu residues

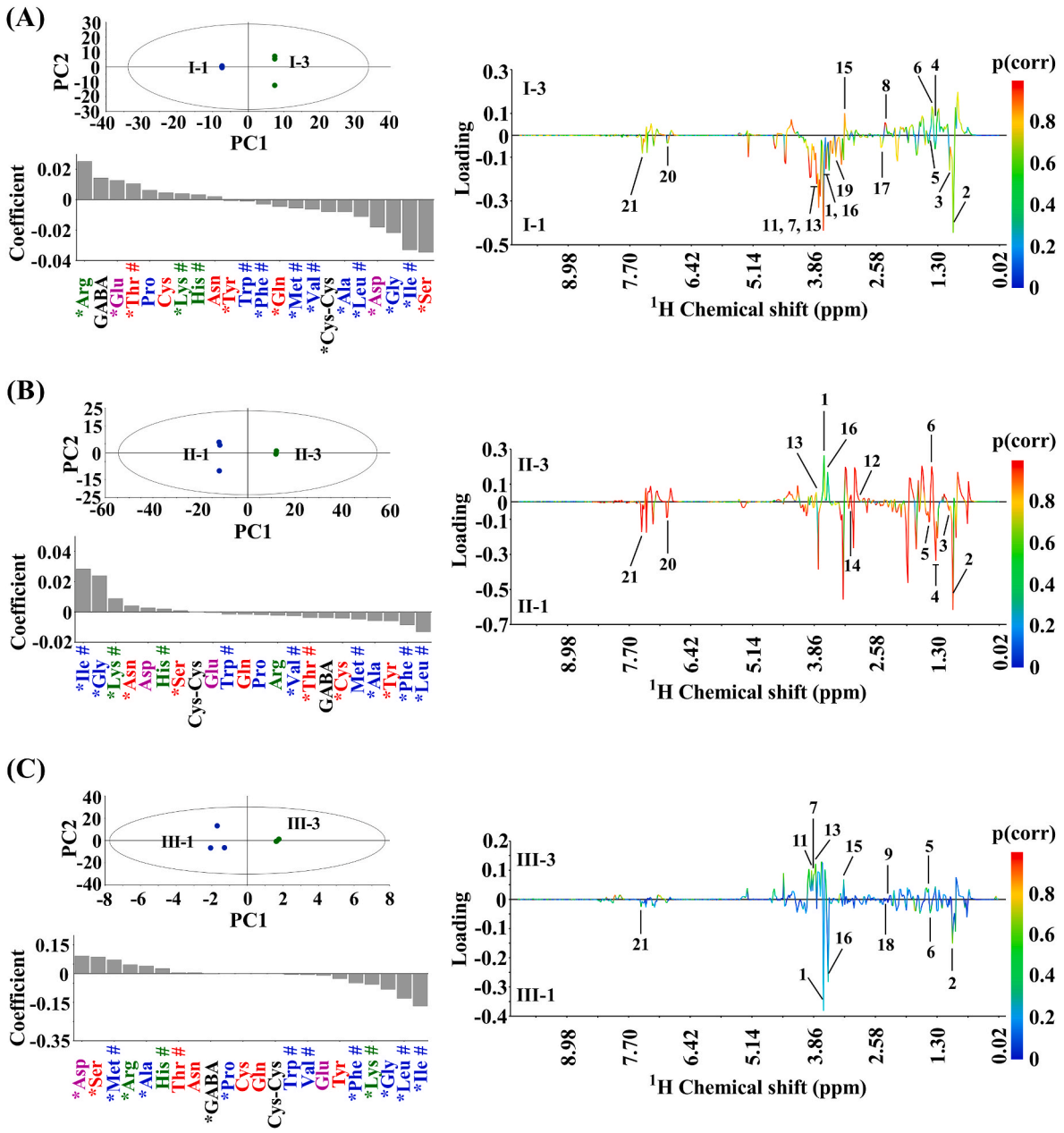

Fig. 7. Orthogonal partial least squares discriminant analysis (OPLS-DA) of pairwise groups. The OPLS-DA score plot, loading S-line plot and OPLS coefficient plot of groups I-1 and I-3 (A), groups II-1 and II-3 (B) and groups III-1 and III-3 (C). Note: I-1: BRPI without MTG treatment; I-3: BRPI with 1 U/g MTG treatment; II-1: PPI without MTG treatment; II-3: PPI with 1 U/g MTG treatment; III-1: BRPI + PPI (4:6) without MTG treatment; III-3: BRPI + PPI (4:6) with 1 U/g MTG treatment. Amino acids marked with an asterisk contribute significantly to the OPLS-DA models (VIP >1). Essential amino acids are marked with pound sign and amino acids in blue, red, green and purple correspond to nonpolar amino acids, polar amino acids with no charge, polar basic amino acids and polar acidic amino acids, respectively. Metabolites keys to the numbers are the same as Table 1.

after MTG treatment, which might be the reason why lower content of Gln and higher content of Glu were shown in our BRPI digesta (Gaspar & de Góes-Favoni, 2015). However, less Lys was observed in MTG-modified BRPI + PPI blend's digests, verifying again that the advanced structures created by MTG in protein-protein associated network could alter the degree of protein degradation in the digestive system as well, accompanied by other changes in the physicochemical properties and secondary structures of protein blend as mentioned above. For essential amino acids, we can see the contents of most of them in all MTG-treated samples were lower than their counterparts without MTG, which was also accordant with previous study (Xing et al., 2016). Thus, the incorporation of MTG into plant protein blends might not only modulate certain biological functions in human body, but also help control the energy intake for losing weight if needed.

4. Conclusion

Although currently soy protein is still dominating the plant-based protein market due to its complete protein profile and good functional properties, its allergic reactions in some individuals can offset brown rice protein's hypoallergenic advantage if blending them together. So we chose pea protein in this study to offer a complementary function to brown rice protein under MTG treatment. The changes of BRPI + PPI's physicochemical properties, such as increased WHC, decreased OHC, reduced solubility and zeta potential in aqueous system, lower gel point temperature and stronger gel strength, could be attributed to the

formation of macromolecular polymers induced by MTG-catalysed crosslinking, which could cause a series of variations in protein's net charge, the distribution of surface amino acids and the network strength. SDS-PAGE results demonstrated that besides isopeptidic bonds, the formation of MTG-induced disulfide bonds also contributed to the generation of large protein polymers with high MW structures. Based on FTIR spectra, more ordered and compact structure with better thermal stability was shown in the 1 U/g MTG-treated BRPI + PPI aggregate, with lower level of RC and higher level of β-sheet structures and α-helix band. NMR-based amino acid profiling showed the advanced structures created by MTG in protein-protein associated network could alter the degree of protein degradation in the digestive system as well, accompanied by less hydrophobic amino acids and essential amino acids released after *in vitro* digestion process. Overall, this study helped us to get a better understanding of MTG's effects on physicochemical properties, protein structural and digestive profile changes of brown rice and pea protein blend, which might contribute to developing novel plant-based meat/seafood analogues in the future. However, some safety concerns of MTG like introducing microbial hazard to foods should be paid attention in practical application.

CRediT authorship contribution statement

Lin Zhao: Conceptualization, Methodology, Investigation, Software, Visualization, Writing-original draft, Writing-review & editing. **Ming-Hsu Chen:** Funding acquisition, Conceptualization, Writing-review. **Xuezhi Bi:** Funding acquisition, Conceptualization. **Juan Du:** Funding acquisition, Conceptualization, Methodology, Project administration, Supervision, Writing-review & editing.

Declaration of competing interest

The authors declare that they have no known competing financial interests or personal relationships that could have appeared to influence the work reported in this paper.

Data availability

Data will be made available on request.

Acknowledgements

This study was funded by Singapore Food Story Theme 2 – 1st Alternative Protein Seed Challenge Grant (W20W2D0013) and Singapore Food Story R&D Programme Industry Alignment Fund Pre-positioning (IAF-PP) Theme 2 – Advanced Biotech-based Protein Production Grant (A21H7a0131 and H21H8a0005). We would like to thank the previous and present lab mates, Ms. Low Li Hui, Mr. Cedric Sow Wee Jian, Ms. Fatin Natasha Binte Abdul Hal, Ms. Zawanah Abdol Rahim Yassin, Ms. Chery Ng Kwoek Zhen, Ms. Felicia Peh Zhi Wen and Mr. Jeremy Chin Tak Gun, for their kindness and assistance.

Appendix A. Supplementary data

Supplementary data to this article can be found online at https://doi.org/10.1016/j.foodhyd.2023.108673.

References

Agboola, S., Ng, D., & Mills, D. (2005). Characterisation and functional properties of Australian rice protein isolates. *Journal of Cereal Science, 41*(3), 283–290.

Amagliani, L., O'Regan, J., Kelly, A. L., & O'Mahony, J. A. (2017). The composition, extraction, functionality and applications of rice proteins: A review. *Trends in Food Science & Technology, 64*, 1–12.

AOAC. (2005). *Official methods of analysis* (18th ed.). Pub AOAC International Maryland.

Barac, M., Cabrilo, S., Pesic, M., Stanojevic, S., Zilic, S., Macej, O., et al. (2010). Profile and functional properties of seed proteins from six pea (*Pisum sativum*) genotypes. *International Journal of Molecular Sciences, 11*(12), 4973–4990.

Bhatty, R. (1982). Albumin proteins of eight edible grain legume species. Electrophoretic patterns and amino acid composition. *Journal of Agricultural and Food Chemistry, 30*(3), 620–622.

Bonet, A., Blaszczak, W., & Rosell, C. M. (2006). Formation of homopolymers and heteropolymers between wheat flour and several protein sources by transglutaminase-catalyzed cross-linking. *Cereal Chemistry, 83*(6), 655–662.

Brodkorb, A., Egger, L., Alminger, M., Alvito, P., Assunção, R., Ballance, S., et al. (2019). INFOGEST static *in vitro* simulation of gastrointestinal food digestion. *Nature Protocols, 14*(4), 991–1014.

Cao, X., Wen, H., Li, C., & Gu, Z. (2009). Differences in functional properties and biochemical characteristics of congenetic rice proteins. *Journal of Cereal Science, 50*(2), 184–189.

Carbonaro, M., Maselli, P., Dore, P., & Nucara, A. (2008). Application of Fourier transform infrared spectroscopy to legume seed flour analysis. *Food Chemistry, 108*(1), 361–368.

Carbonaro, M., Maselli, P., & Nucara, A. (2012). Relationship between digestibility and secondary structure of raw and thermally treated legume proteins: A fourier transform infrared (FT-IR) spectroscopic study. *Amino Acids, 43*(2), 911–921.

Casey, R. (1982). The genetics of pea seed storage proteins. *Plant Foods for Human Nutrition, 31*(3), 281–295.

Chan, F. T., Pinotsi, D., Gabriele, S., Schierle, K., & Kaminski, C. F. (2014). Structure-specific intrinsic fluorescence of protein amyloids used to study their kinetics of aggregation. In V. N. Uversky, & Y. L. Lyubchenko (Eds.), *Bio-nanoimaging* (pp. 147–155). Academic Press.

DeJong, G., & Koppelman, S. (2002). Transglutaminase catalyzed reactions: Impact on food applications. *Journal of Food Science, 67*(8), 2798–2806.

Djoullah, A., Djemaoune, Y., Husson, F., & Saurel, R. (2015). Native-state pea albumin and globulin behavior upon transglutaminase treatment. *Process Biochemistry, 50*(8), 1284–1292.

Dube, M., Schäfer, C., Neidhart, S., & Carle, R. (2007). Texturisation and modification of vegetable proteins for food applications using microbial transglutaminase. *European Food Research and Technology, 225*(2), 287–299.

Du, J., Reuhs, B. L., & Jones, O. G. (2016). Influence of PEGylation on the ability of carboxymethyl-dextran to form complexes with α-lactalbumin. *Food Chemistry, 196*, 853–859.

Fang, M., Xiong, S., Hu, Y., Yin, T., & You, J. (2019). *In vitro* pepsin digestion of silver carp (*Hypophthalmichthys molitrix*) surimi gels after cross-linking by Microbial Transglutaminase (MTGase). *Food Hydrocolloids, 95*, 152–160.

Gaspar, A. L. C., & de Góes-Favoni, S. P. (2015). Action of microbial transglutaminase (MTGase) in the modification of food proteins: A review. *Food Chemistry, 171*, 315–322.

Glusac, J., Isaschar-Ovdat, S., & Fishman, A. (2020). Transglutaminase modifies the physical stability and digestibility of chickpea protein-stabilized oil-in-water emulsions. *Food Chemistry, 315*, Article 126301.

Gorissen, S. H., Crombag, J. J., Senden, J. M., Waterval, W., Bierau, J., Verdijk, L. B., et al. (2018). Protein content and amino acid composition of commercially available plant-based protein isolates. *Amino Acids, 50*(12), 1685–1695.

He, C., Hu, Y., Woo, M. W., Xiong, H., & Zhao, Q. (2021). Effect of microbial transglutaminase on the structural and rheological characteristics and *in vitro* digestion of rice glutelin–casein blends. *Food Research International, 139*, Article 109832.

Herz, E. M., Schäfer, S., Terjung, N., Gibis, M., & Weiss, J. (2021). Influence of transglutaminase on glucono-δ-lactone-induced soy protein gels. *ACS Food Science & Technology, 1*(8), 1412–1417.

He, Y., Zhao, X., Chen, L., Zhao, L., & Yang, H. (2021). Effect of electrolysed water generated by sodium chloride combined with sodium bicarbonate solution against *Listeria innocua* in broth and on shrimp. *Food Control, 127*, Article 108134.

Huang, M., Mao, Y., Li, H., & Yang, H. (2021). Kappa-carrageenan enhances the gelation and structural changes of egg yolk via electrostatic interactions with yolk protein. *Food Chemistry, 360*, Article 129972.

Ikujenlola, V. A., & Fashakin, J. B. (2005). The physico-chemical properties of a complementary diet prepared from vegetable proteins. *Journal of Food Agriculture and Environment, 3*(3/4), 23.

Jiang, S., Ding, J., Andrade, J., Rababah, T. M., Almajwal, A., Abulmeaty, M. M., et al. (2017). Modifying the physicochemical properties of pea protein by pH-shifting and ultrasound combined treatments. *Ultrasonics Sonochemistry, 38*, 835–842.

Jiménez-Munoz, L. M., Tavares, G. M., & Corredig, M. (2021). Design future foods using plant protein blends for best nutritional and technological functionality. *Trends in Food Science & Technology, 113*, 139–150.

Kalman, D. S. (2014). Amino acid composition of an organic brown rice protein concentrate and isolate compared to soy and whey concentrates and isolates. *Foods, 3*(3), 394–402.

Kruger, N. J. (2009). The Bradford method for protein quantitation. *The Protein Protocols Handbook*, 17–24.

Kumar, M., Tomar, M., Potkule, J., Reetu, Punia, S., Dhakane-Lad, J., et al. (2022). Functional characterization of plant-based protein to determine its quality for food applications. *Food Hydrocolloids, 123*, Article 106986.

Kupkanchanakul, W., Kadowaki, M., Kubota, M., & Naivikul, O. (2018). Effect of pre-germination at varying stages of embryonic growth length on chemical composition and protein profile of Thai rice (*Oryza sativa* L.). *Agriculture and Natural Resources, 52*(1), 59–65.

Lerner, A., & Matthias, T. (2019). Microbial transglutaminase is beneficial to food industries but a caveat to public health. *Med One, 4*(1), Article e190001.

Li, J., Fu, J., Ma, Y., He, Y., Fu, R., Qayum, A., et al. (2022). Low temperature extrusion promotes transglutaminase cross-linking of whey protein isolate and enhances its

emulsifying properties and water holding capacity. *Food Hydrocolloids, 125*, Article 107410.
Liu, M., & Damodaran, S. (1999). Effect of transglutaminase-catalyzed polymerization of β-casein on its emulsifying properties. *Journal of Agricultural and Food Chemistry, 47*(4), 1514–1519.
Lu, Z., Lee, P.-R., & Yang, H. (2022). Chickpea flour and soy protein isolate interacted with κ-carrageenan via electrostatic interactions to form egg omelets analogue. *Food Hydrocolloids, 130*, Article 107691.
Malhotra, A., & Coupland, J. N. (2004). The effect of surfactants on the solubility, zeta potential, and viscosity of soy protein isolates. *Food Hydrocolloids, 18*(1), 101–108.
Marco, C., Pérez, G., Ribotta, P., & Rosell, C. M. (2007). Effect of microbial transglutaminase on the protein fractions of rice, pea and their blends. *Journal of the Science of Food and Agriculture, 87*(14), 2576–2582.
Mills, E. C., Marigheto, N. A., Wellner, N., Fairhurst, S. A., Jenkins, J. A., Mann, R., et al. (2003). Thermally induced structural changes in glycinin, the 11S globulin of soya bean (*Glycine max*)—an in situ spectroscopic study. *Biochimica et Biophysica Acta, Proteins and Proteomics, 1648*(1–2), 105–114.
Minekus, M., Alminger, M., Alvito, P., Ballance, S., Bohn, T., Bourlieu, C., et al. (2014). A standardised static *in vitro* digestion method suitable for food–an international consensus. *Food & Function, 5*(6), 1113–1124.
Monogioudi, E., Faccio, G., Lille, M., Poutanen, K., Buchert, J., & Mattinen, M.-L. (2011). Effect of enzymatic cross-linking of β-casein on proteolysis by pepsin. *Food Hydrocolloids, 25*(1), 71–81.
Moreno, H. M., Tovar, C. A., Dominguez-Timon, F., Cano-Baez, J., Díaz, M. T., Pedrosa, M. M., et al. (2020). Gelation of commercial pea protein isolate: Effect of microbial transglutaminase and thermal processing. *Food Science and Technology, 40*, 800–809.
Nasrabadi, M. N., Doost, A. S., & Mezzenga, R. (2021). Modification approaches of plant-based proteins to improve their techno-functionality and use in food products. *Food Hydrocolloids, 118*, Article 106789.
Netrprachit, P., Ogawa, M., & Suwannaporn, P. (2019). Transglutaminase crosslinking to improve quality of rice flour gel. *Italian Journal of Food Science, 31*(5), 163–170.
Qin, X. S., Luo, S. Z., Cai, J., Zhong, X. Y., Jiang, S. T., Zhao, Y. Y., et al. (2016). Transglutaminase-induced gelation properties of soy protein isolate and wheat gluten mixtures with high intensity ultrasonic pretreatment. *Ultrasonics Sonochemistry, 31*, 590–597.
Renzetti, S., Behr, J., Vogel, R., & Arendt, E. (2008). Transglutaminase polymerisation of buckwheat (*Fagopyrum esculentum* Moench) proteins. *Journal of Cereal Science, 48*(3), 747–754.
Shen, Y., Hong, S., Singh, G., Koppel, K., & Li, Y. (2022). Improving functional properties of pea protein through "green" modifications using enzymes and polysaccharides. *Food Chemistry, 385*, Article 132687.
Shen, Y., & Li, Y. (2021). Acylation modification and/or guar gum conjugation enhanced functional properties of pea protein isolate. *Food Hydrocolloids, 117*, Article 106686.
Shen, Y., Tang, X., & Li, Y. (2021). Drying methods affect physicochemical and functional properties of quinoa protein isolate. *Food Chemistry, 339*, Article 127823.
Solovyev, A. Y., Tarnovskaya, S. I., Chernova, I. A., Shataeva, L. K., & Skorik, Y. A. (2015). The interaction of amino acids, peptides, and proteins with DNA. *International Journal of Biological Macromolecules, 78*, 39–45.
Sow, L. C., & Yang, H. (2015). Effects of salt and sugar addition on the physicochemical properties and nanostructure of fish gelatin. *Food Hydrocolloids, 45*, 72–82.
Sun, X. D., & Arntfield, S. D. (2010). Gelation properties of salt-extracted pea protein induced by heat treatment. *Food Research International, 43*(2), 509–515.
Tang, C.-H., & Sun, X. (2011). A comparative study of physicochemical and conformational properties in three vicilins from *Phaseolus* legumes: Implications for the structure–function relationship. *Food Hydrocolloids, 25*(3), 315–324.
Tang, C.-H., Wu, H., Chen, Z., & Yang, X.-Q. (2006). Formation and properties of glycinin-rich and β-conglycinin-rich soy protein isolate gels induced by microbial transglutaminase. *Food Research International, 39*(1), 87–97.
Truong, V. D., Clare, D. A., Catignani, G. L., & Swaisgood, H. E. (2004). Cross-linking and rheological changes of whey proteins treated with microbial transglutaminase. *Journal of Agricultural and Food Chemistry, 52*(5), 1170–1176.
Villar-Piqué, A., Sabaté, R., Lopera, O., Gibert, J., Torne, J. M., Santos, M., et al. (2010). Amyloid-like protein inclusions in tobacco transgenic plants. *PLoS One, 5*(10), Article e13625.
Wang, C., Li, T., Ma, L., Li, T., Yu, H., Hou, J., et al. (2020). Consequences of superfine grinding treatment on structure, physicochemical and rheological properties of transglutaminase-crosslinked whey protein isolate. *Food Chemistry, 309*, Article 125757.
Wang, Y., Ning, Y., Yuan, C., Cui, B., Liu, G., & Zhang, Z. (2021). The protective mechanism of a debranched corn starch/konjac glucomannan composite against dyslipidemia and gut microbiota in high-fat-diet induced type 2 diabetes. *Food & Function, 12*(19), 9273–9285.
Wang, W., Zhong, Q., & Hu, Z. (2013). Nanoscale understanding of thermal aggregation of whey protein pretreated by transglutaminase. *Journal of Agricultural and Food Chemistry, 61*(2), 435–446.
Wilcox, C. P., Clare, D. A., Valentine, V. W., & Swaisgood, H. E. (2002). Immobilization and utilization of the recombinant fusion proteins trypsin−streptavidin and streptavidin− transglutaminase for modification of whey protein isolate functionality. *Journal of Agricultural and Food Chemistry, 50*(13), 3723–3730.
Wilcox, C. P., & Swaisgood, H. E. (2002). Modification of the rheological properties of whey protein isolate through the use of an immobilized microbial transglutaminase. *Journal of Agricultural and Food Chemistry, 50*(20), 5546–5551.
Withana-Gamage, T. S., Wanasundara, J. P., Pietrasik, Z., & Shand, P. J. (2011). Physicochemical, thermal and functional characterisation of protein isolates from kabuli and desi chickpea (*Cicer arietinum* L.): A comparative study with soy (*Glycine max*) and pea (*Pisum sativum* L.). *Journal of the Science of Food and Agriculture, 91*(6), 1022–1031.
Wu, J., Zhao, L., Lai, S., & Yang, H. (2021). NMR-based metabolomic investigation of antimicrobial mechanism of electrolysed water combined with moderate heat treatment against *Listeria monocytogenes* on salmon. *Food Control, 125*, Article 107974.
Xing, G., Rui, X., Jiang, M., Xiao, Y., Guan, Y., Wang, D., et al. (2016). *In vitro* gastrointestinal digestion study of a novel bio-tofu with special emphasis on the impact of microbial transglutaminase. *PeerJ, 4*, Article e2754.
Yildirim, M., Hettiarachchy, N., & Kalapathy, U. (1996). Properties of biopolymers from cross-linking whey protein isolate and soybean 11S globulin. *Journal of Food Science, 61*(6), 1129–1132.
Yu, P. (2005). Protein secondary structures (α-helix and β-sheet) at a cellular level and protein fractions in relation to rumen degradation behaviours of protein: A new approach. *British Journal of Nutrition, 94*(5), 655–665.
Zhang, P., Hu, T., Feng, S., Xu, Q., Zheng, T., Zhou, M., et al. (2016). Effect of high intensity ultrasound on transglutaminase-catalyzed soy protein isolate cold set gel. *Ultrasonics Sonochemistry, 29*, 380–387.
Zhang, W., Zhao, P., Li, J., Wang, X., Hou, J., & Jiang, Z. (2022). Effects of ultrasound synergized with microwave on structure and functional properties of transglutaminase-crosslinked whey protein isolate. *Ultrasonics Sonochemistry, 83*, Article 105935.
Zhao, L., Poh, C. N., Wu, J., Zhao, X., He, Y., & Yang, H. (2022). Effects of electrolysed water combined with ultrasound on inactivation kinetics and metabolite profiles of *Escherichia coli* biofilms on food contact surface. *Innovative Food Science & Emerging Technologies, 76*, Article 102917.
Zhao, L., Zhao, M. Y., Phey, C. P., & Yang, H. (2019). Efficacy of low concentration acidic electrolysed water and levulinic acid combination on fresh organic lettuce (*Lactuca sativa* Var. *Crispa* L.) and its antimicrobial mechanism. *Food Control, 101*, 241–250.
Zhao, L., Zhao, X., Wu, J.e., Lou, X., & Yang, H. (2019). Comparison of metabolic response between the planktonic and air-dried *Escherichia coli* to electrolysed water combined with ultrasound by ^{1}H NMR spectroscopy. *Food Research International, 125*, Article 108607.
Zhu, S. M., Lin, S. L., Ramaswamy, H. S., Yu, Y., & Zhang, Q. T. (2017). Enhancement of functional properties of rice bran proteins by high pressure treatment and their correlation with surface hydrophobicity. *Food and Bioprocess Technology, 10*(2), 317–327.